Supporting Information

Mineralization enhancement of pharmaceutical contaminants by radical-based oxidation promoted by oxide-bound metal ions

Mahamadou Kamagate[1, 2], Mathieu Pasturel[3], Marcello Brigante[4], Khalil Hanna[*1,5]

[1]Univ Rennes, École Nationale Supérieure de Chimie de Rennes, UMR CNRS 6226, 11 Allée de Beaulieu, F-35708 Rennes Cedex 7, France.

[2]Université de Man, BP 20 Man, Côte d'Ivoire.

[3]Univ Rennes, Université de Rennes 1, UMR CNRS 6226, Avenue General Leclerc, F-35708 Rennes Cedex 7, France.

[4]Université Clermont Auvergne, CNRS, SIGMA Clermont, Institut de Chimie de Clermont-Ferrand, F-63000 Clermont–Ferrand, France.

[5] Institut Universitaire de France (IUF), MESRI, 1 rue Descartes, 75231 Paris Cedex.

*Corresponding author: khalil.hanna@ensc-rennes.fr / +332 23 23 80 27

Revised manuscript to *Environmental Science & Technology*

December, 2019

21 Pages, 16 Figures, 3 Tables

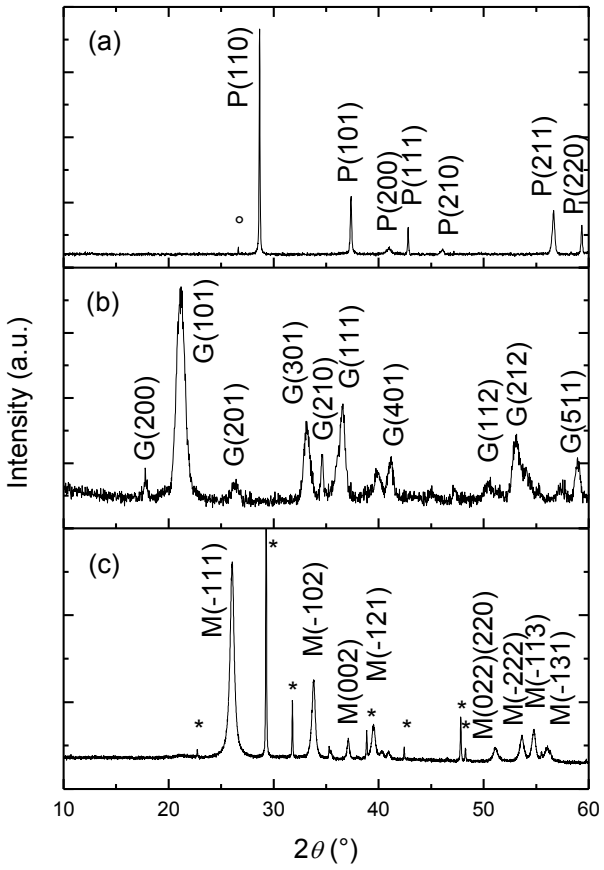

Figure S1. XRD patterns of the starting materials used in this study: (a) MnO_2 indexed with the pyrolusite structure (° indicate an impurity peak probably belonging to MnOOH); (b) FeOOH indexed with the goethite structure; (c) MnOOH indexed with the manganite structure (* indicates an XRD contribution from the stored salt $NaNO_3$ of manganite suspension). For clarity, only the main Bragg peaks are indexed.

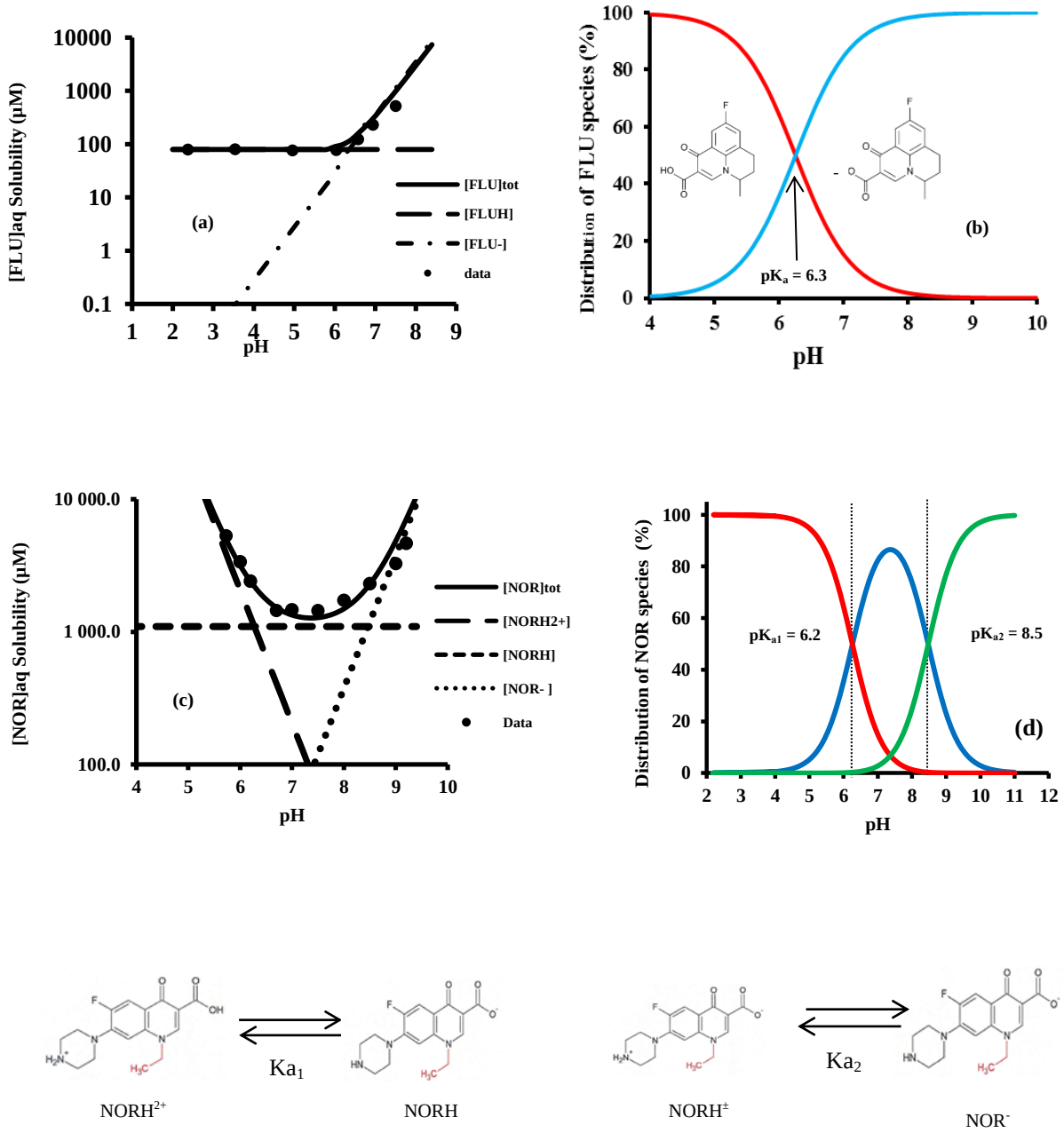

Figure S2. Solubility and distribution of species of FLU (a, b) and NOR (c, d), respectively.

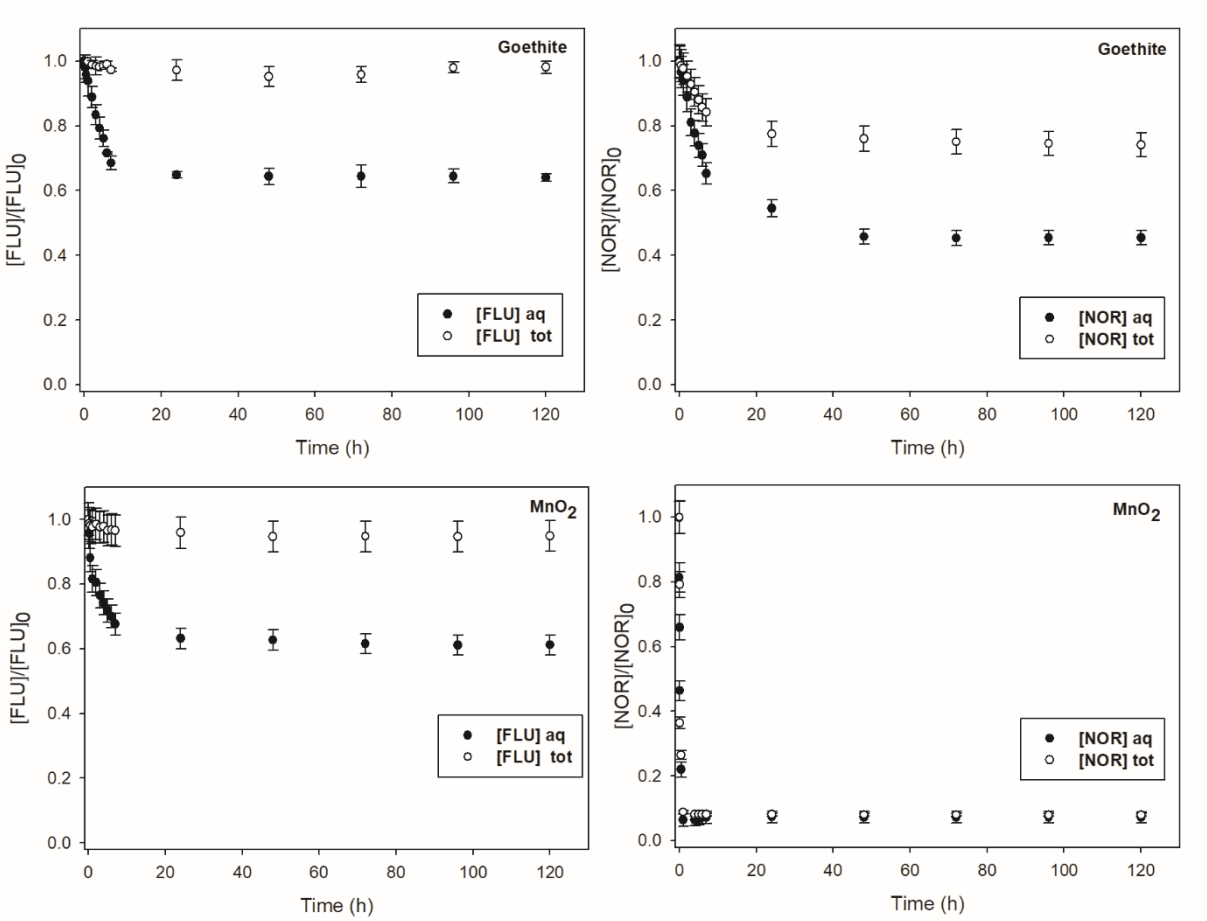

Figure S3. Removal kinetics of FLU (24 µM) and NOR (24 µM) onto 10 m^2 L^{-1} α-FeOOH or MnO_2 under dark conditions at pH = 6.5 ± 0.1. aq = aqueous residual concentration; tot = total concentration representing both aqueous (residual) and adsorbed concentrations.

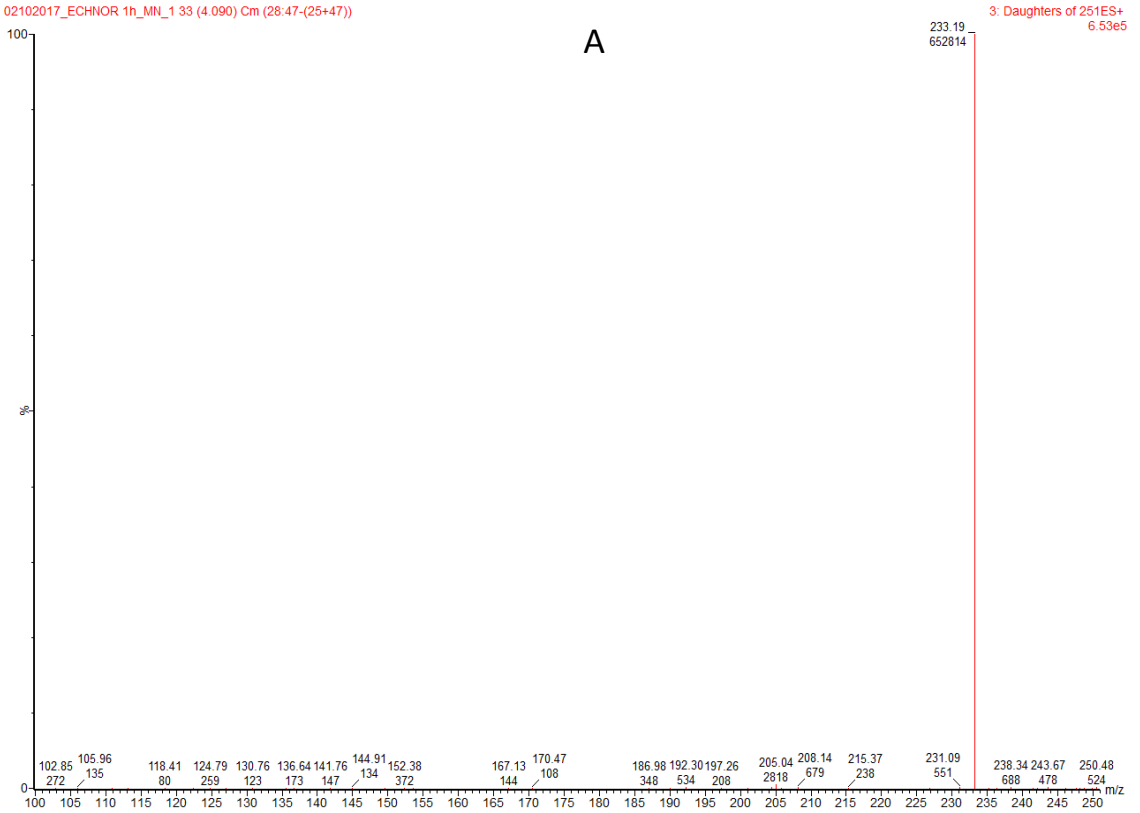
02102017_ECHNOR 1h_MN_1 33 (4.090) Cm (28:47-(25+47))
3: Daughters of 251ES+
6.53e5
A
233.19
652814
100
%
0
102.85 272
105.96 135
118.41 80
124.79 259
130.76 123
136.64 173
141.76 147
144.91 134
152.38 372
167.13 144
170.47 108
186.98 348
192.30 534
197.26 208
205.04 2818
208.14 679
215.37 238
231.09 551
238.34 688
243.67 478
250.48 524
m/z

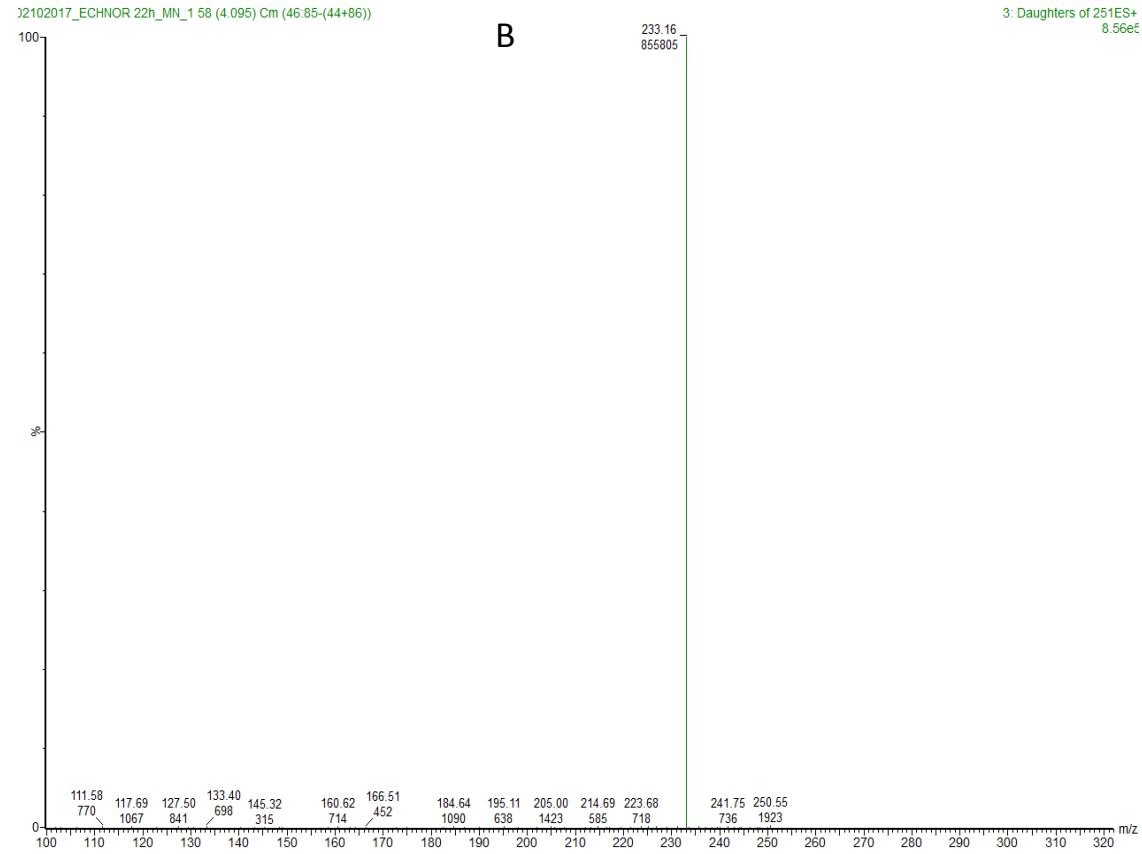
02102017_ECHNOR 22h_MN_1 58 (4.095) Cm (46:85-(44+86))
3: Daughters of 251ES+
8.56e5
B
233.16
855805
100
%
0
111.58 770
117.69 1067
127.50 841
133.40 698
145.32 315
160.62 714
166.51 452
184.64 1090
195.11 638
205.00 1423
214.69 585
223.68 718
241.75 736
250.55 1923
m/z

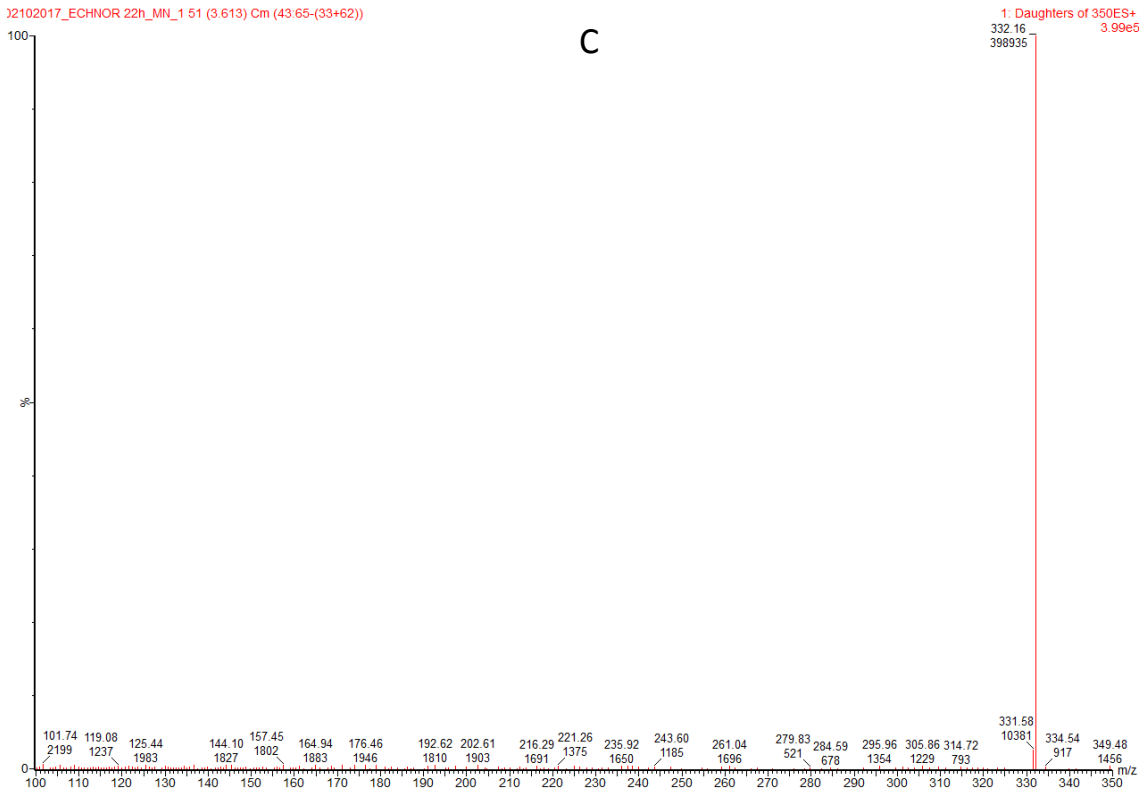

Figure S4. UHPLC-ESI-MS spectra of oxidation products of Norfloxacin at pH 6.5 $[NOR]_o$ = 24 µM; $[MnO_2]_o$ = 0,027g L^{-1} (10 m^2 L^{-1}); Pre-equilibrium time 1h (A) and 22 h (B and C).

Scheme S1: possible oxidation pathways of NOR.

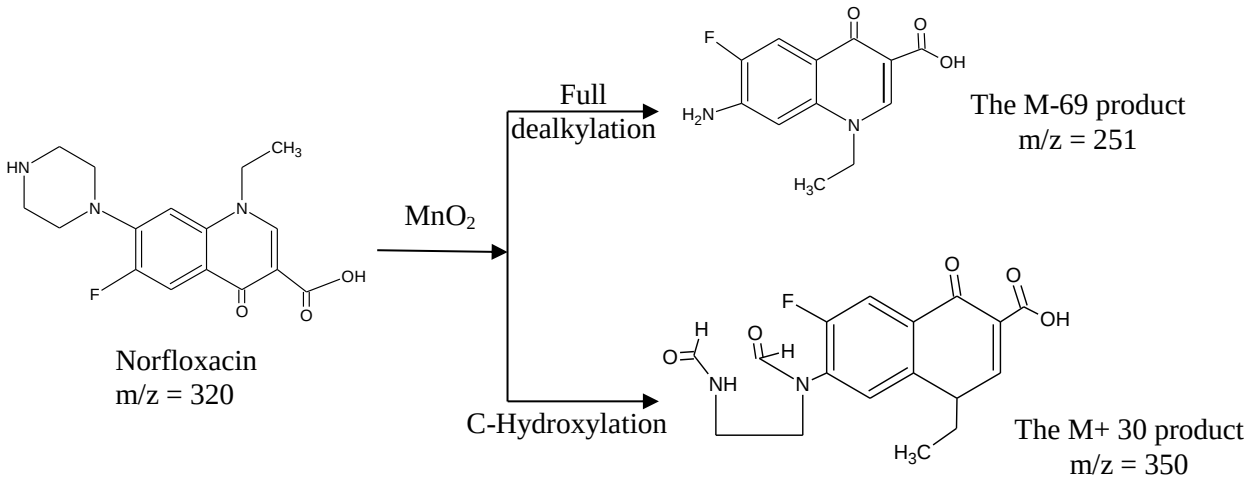

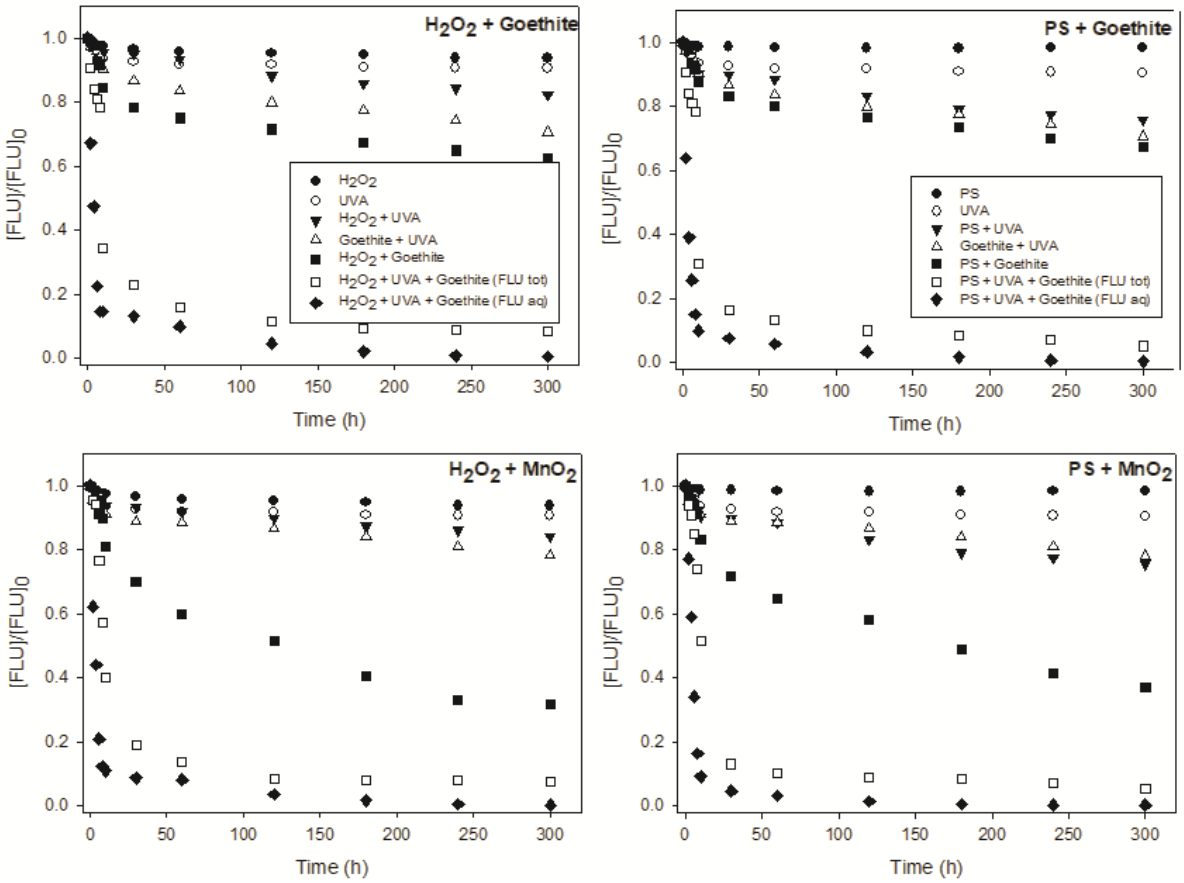

Figure S5. Removal kinetics of FLU under dark and irradiation conditions at pH 6.5 ± 0.1: $[FLU]_o$ = 24 µM; $[H_2O_2]_o = [S_2O_8^{2-}]_o$ = 0.5 mM; [goethite]$_o$ = 0.118 g L^{-1} (10 m^2/L); $[MnO_2]_o$ = 0.027g L^{-1} (10 m^2 L^{-1}); aq = aqueous residual concentration; tot = total concentration representing both aqueous (residual) and adsorbed concentrations. The same legend is valid for goethite or MnO_2.

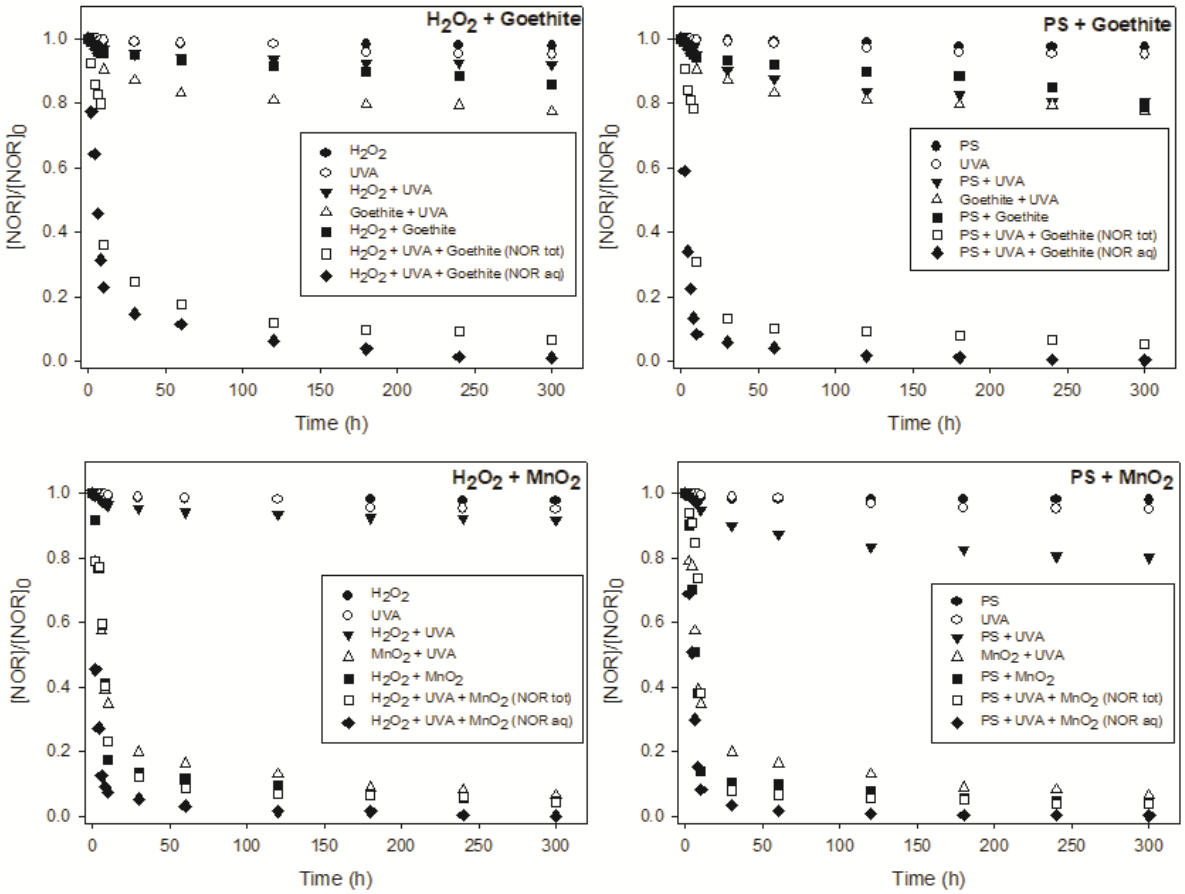

Figure S6. Removal kinetics of NOR under dark and irradiation conditions at pH 6.5 ± 0.1: $[NOR]_o$ = 24 µM; $[H_2O_2]_o$ = $[S_2O_8^{2-}]_o$ = 0.5 mM; [goethite]$_o$ = 0.118g L^{-1} (10 m^2 L^{-1}); $[MnO_2]_o$ = 0.027g L^{-1} (10 m^2 L^{-1}). aq = aqueous residual concentration; tot = total concentration representing both aqueous (residual) and adsorbed concentrations.

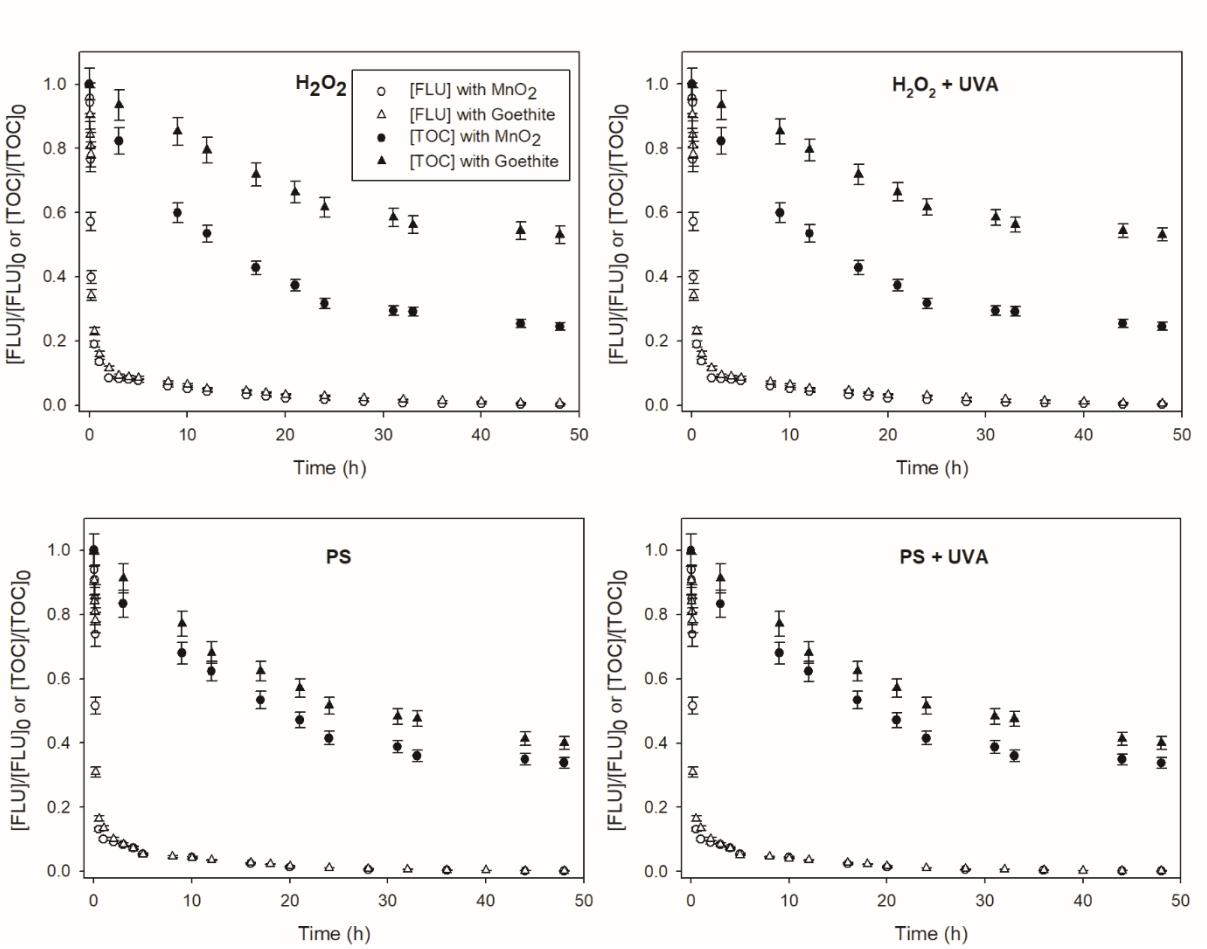

Figure S7. Removal kinetics of FLU_{tot} (empty symbols) and TOC_{tot} (full symbols) under dark and irradiation conditions at pH 6.5 ± 0.1: $[FLU]_o$ = 24 µM; $[H_2O_2]_o$ = $[S_2O_8^{2-}]_o$ = 0.5 mM; $[goethite]_o$ = 0.118g L^{-1} (10 m^2 L^{-1}); $[MnO_2]_o$ = 0.027g L^{-1} (10 m^2 L^{-1}).

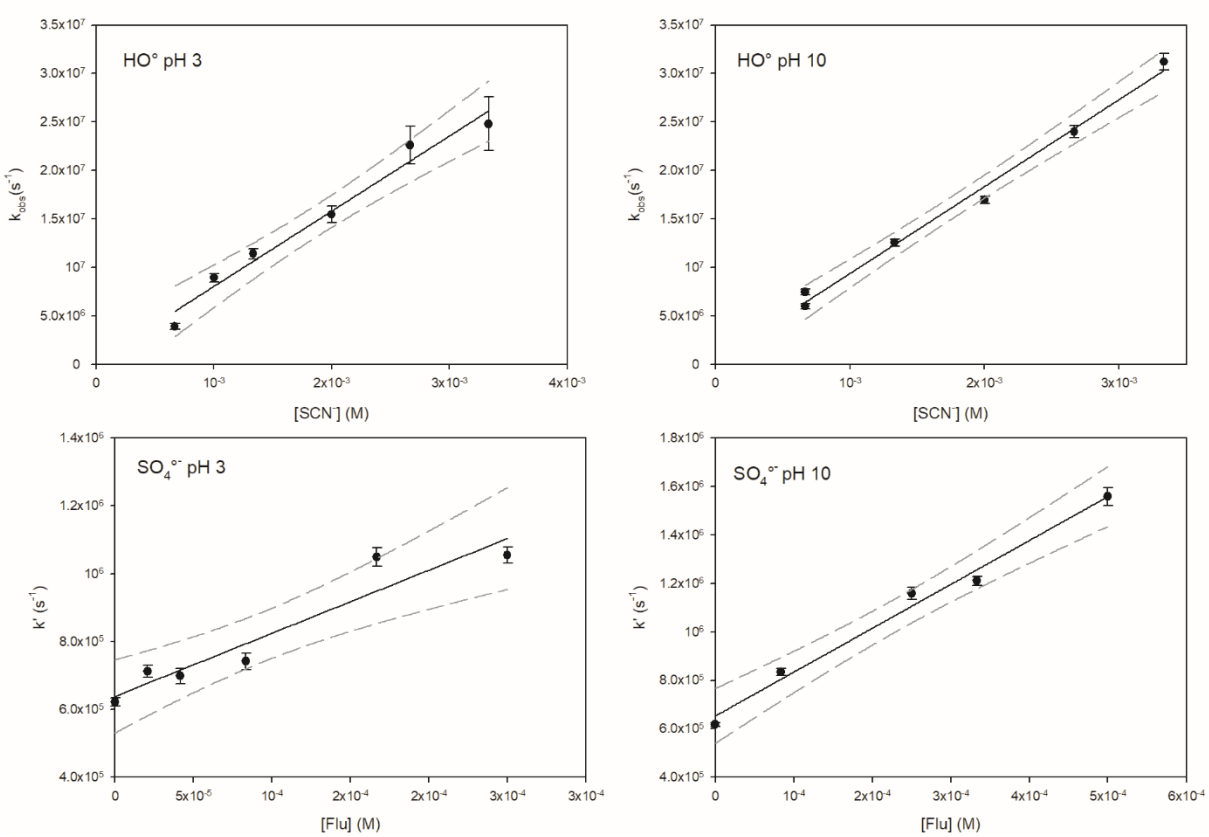

Figure S8. Determination of FLU reactivity with hydroxyl radical using competition kinetics with thiocyanate anion (SCN^-) at pH 3 and 10.

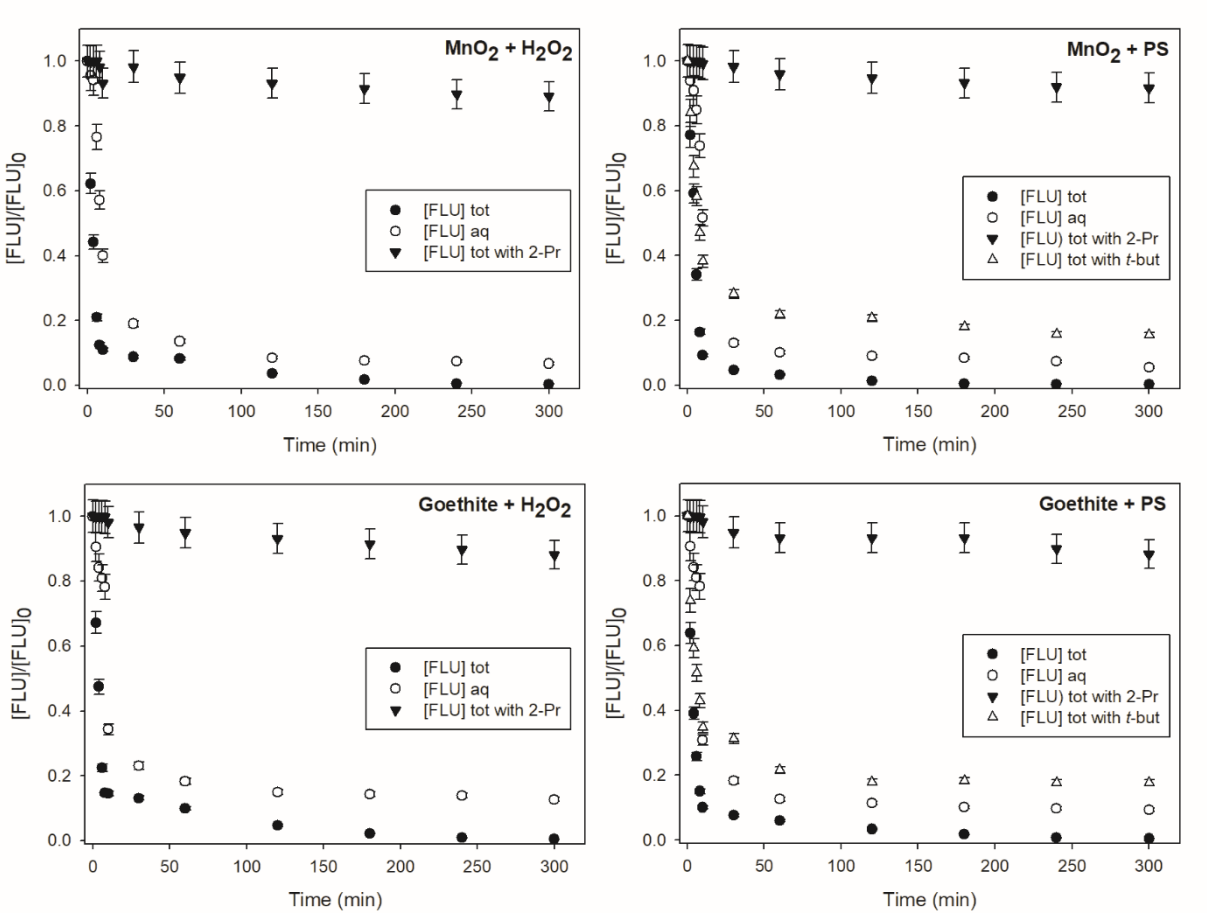

Figure S9. Scavenger tests for UVA + goethite or MnO_2 + H_2O_2 or $S_2O_8^{2-}$ (PS)) at pH 6.5 ± 0.1: [FLU] = 24 µM; [H_2O_2] = [$S_2O_8^{2-}$] = 0.5 mM; [goethite] = [MnO_2] = 10 m²/L; [2-Pr] = 100 mM; [*t*-but]=10 mM; reaction time =300 min.

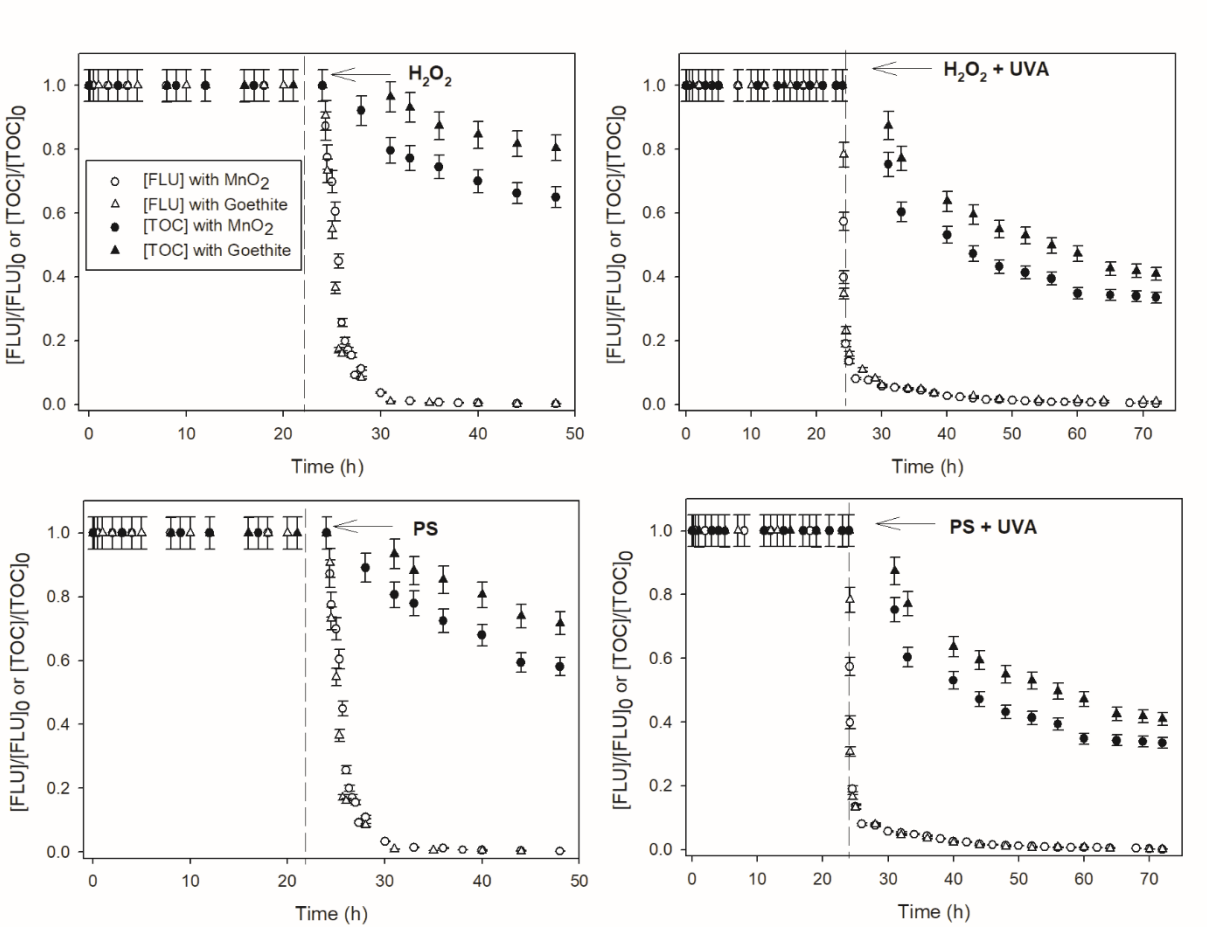

Figure S10. Removal kinetics of FLU_{tot} (empty symbols) and TOC_{tot} (full symbols) with 24 h of pre-equilibration time before addition of oxidants, under dark and irradiation conditions and at pH 6.5 ± 0.1: $[FLU]_o$ = 24 µM; $[S_2O_8^{2-}]_o$ = 0.5 mM; $[MnO_2]_o$ = 0.027g L^{-1} (10 m^2 L^{-1}); h. The arrow indicates the moment where oxidant addition and/or UVA irradiation take place.

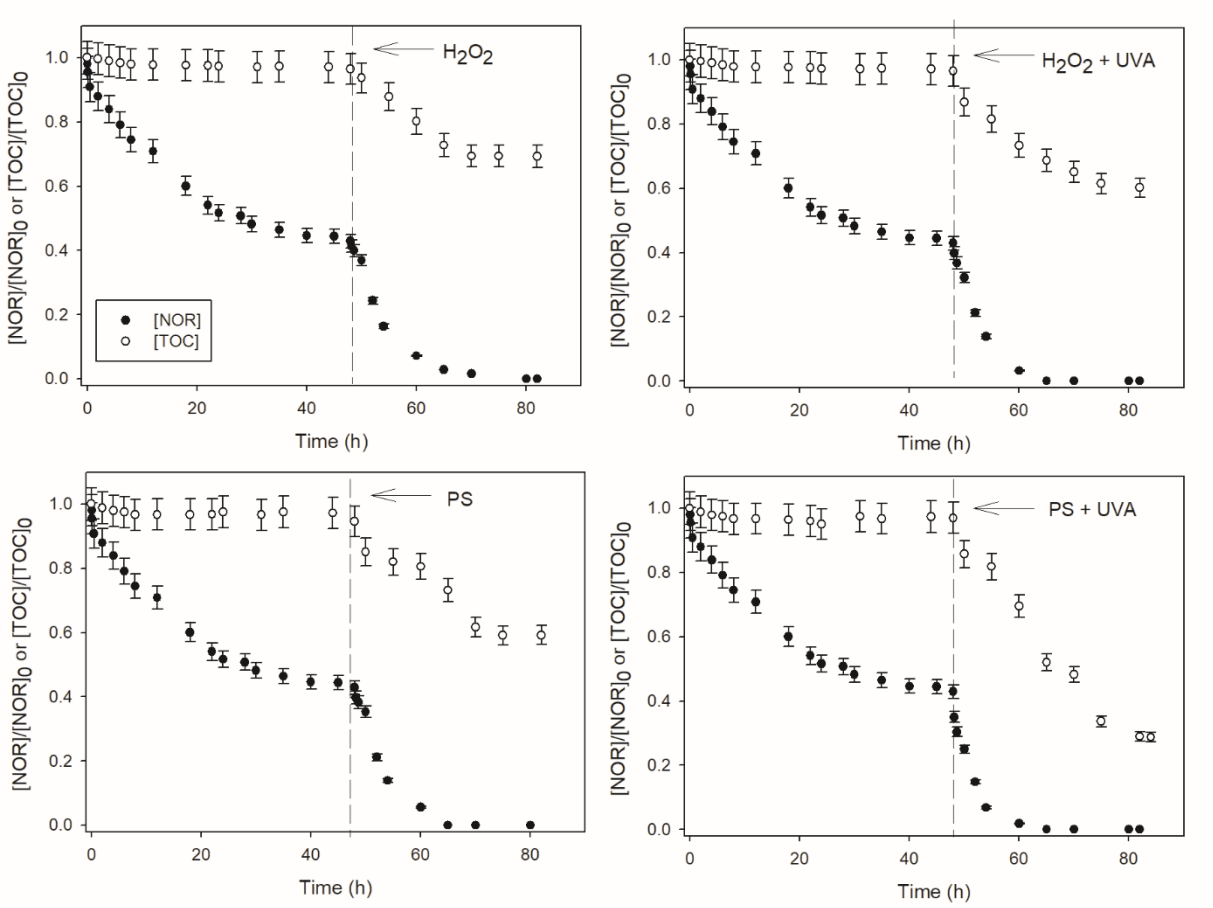

Figure S11. Removal kinetics of NOR_{tot} (full symbols) and TOC_{tot} (empty symbols) under dark and irradiation conditions at pH 6.5 ± 0.1: $[NOR]_o$ = 24 µM; $[H_2O_2]_o = [S_2O_8^{2-}]_o$ = 0.5 mM; $[goethite]_o$ = 0.118g L^{-1} (10 m^2 L^{-1}); Pre-equilibration time = 48 h; The arrow indicates the moment where oxidant addition and/or UVA irradiation take place.

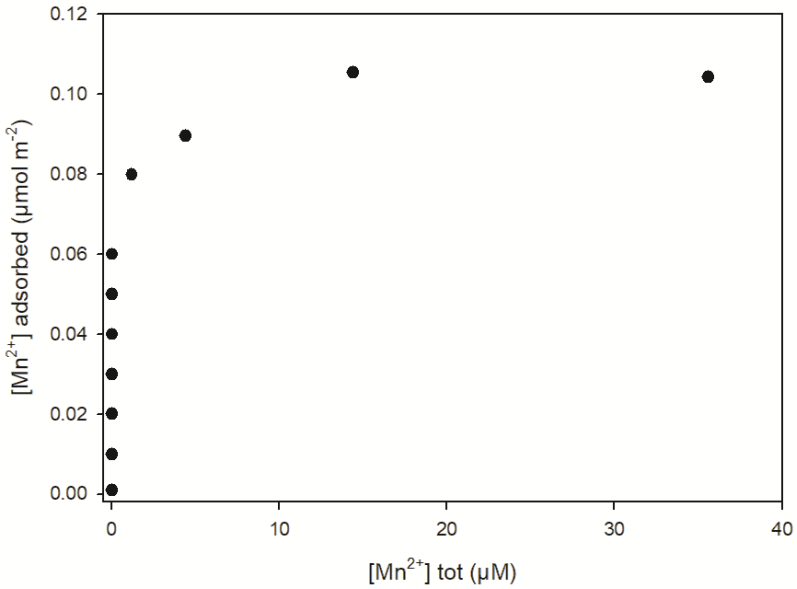

Figure S12. Adsorption isotherm of Mn^{2+} on MnO_2 at pH 6.5 ± 0.1: $[MnO_2]_o$ = 0.027g L^{-1} (10 m^2 L^{-1}); $[Mn^{2+}]_{initial}$ = 0 - 140 µM; reaction time = 48h.

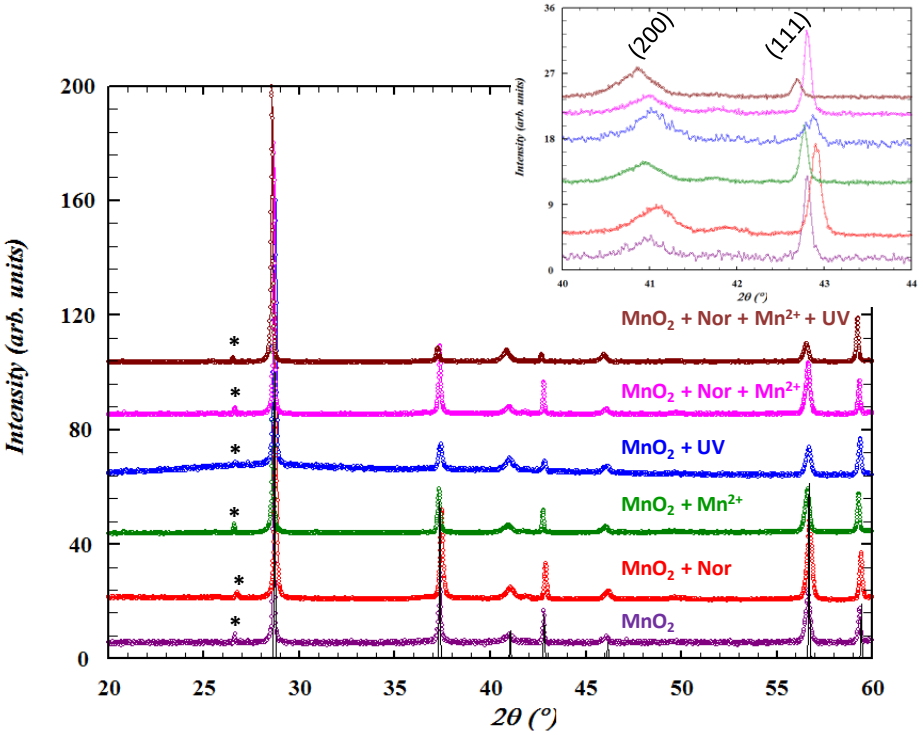

Figure S13. Powder XRD patterns (shifted along z for clarity) of unreacted MnO_2 (purple) and MnO_2 reacted in different processes after 72 h of reaction time. The theoretical XRD pattern of tetragonal MnO_2 is plotted in black solid line and the asterisks indicate the probable highest intensity peak of γ-MnO(OH). The inset shows a zoomed area evidencing the intensity ratio change between (200) and (111) Bragg peaks of pyrolusite when MnO_2 is irradiated with UV light (blue and brown symbols, see text for details). The observed peak shift, which is related to the "zero-shift" of the measurements performed on various sample holders, is considered during Rietveld refinements.

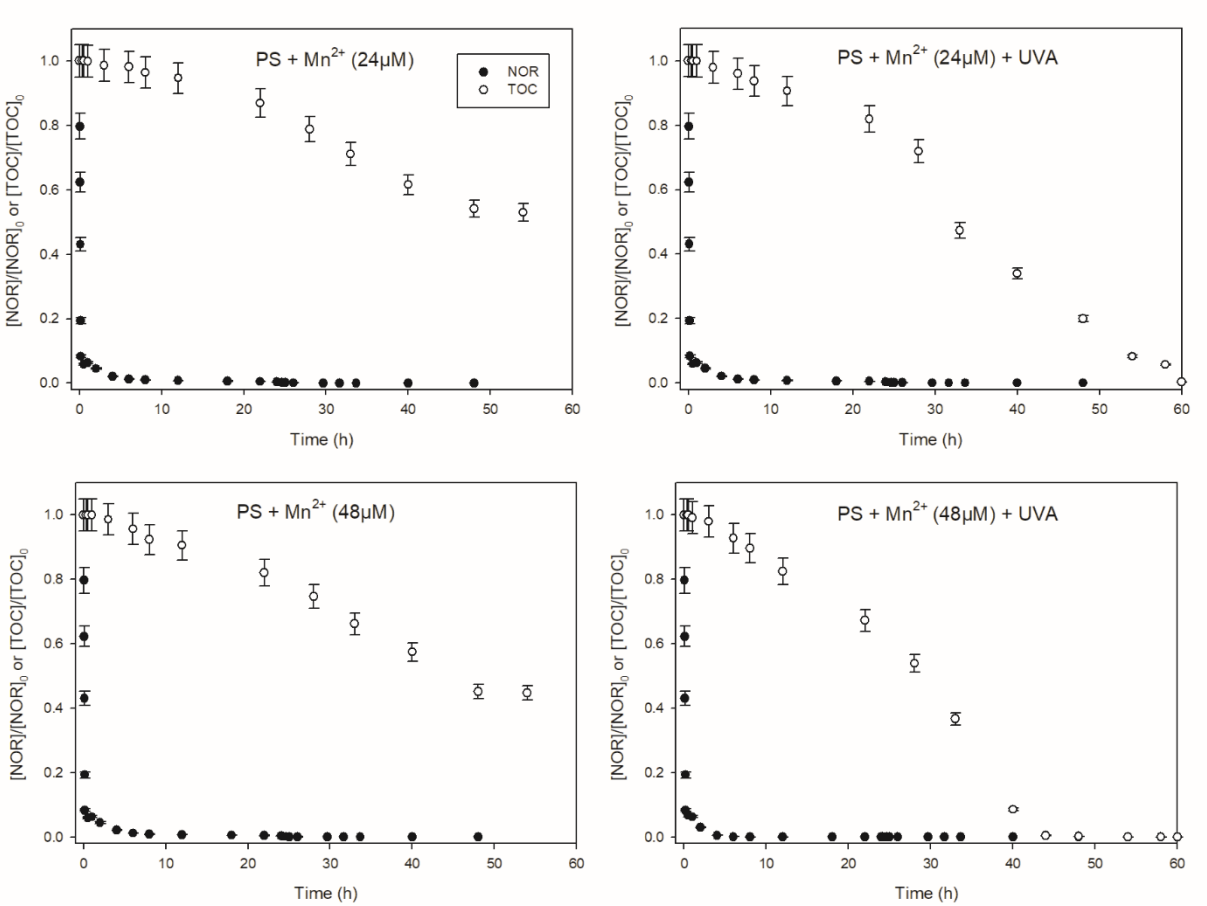

Figure S14. Removal kinetics of NOR_{tot} (full symbols) and TOC_{tot} (empty symbols) in presence of Mn^{2+} under dark and irradiation conditions and at pH 6.5 ± 0.1: $[NOR]_o$ = 24 µM; $[S_2O_8^{2-}]_o$ = 0.5 mM; $[MnO_2]_o$ = 0.027g L^{-1} (10 m^2 L^{-1}).

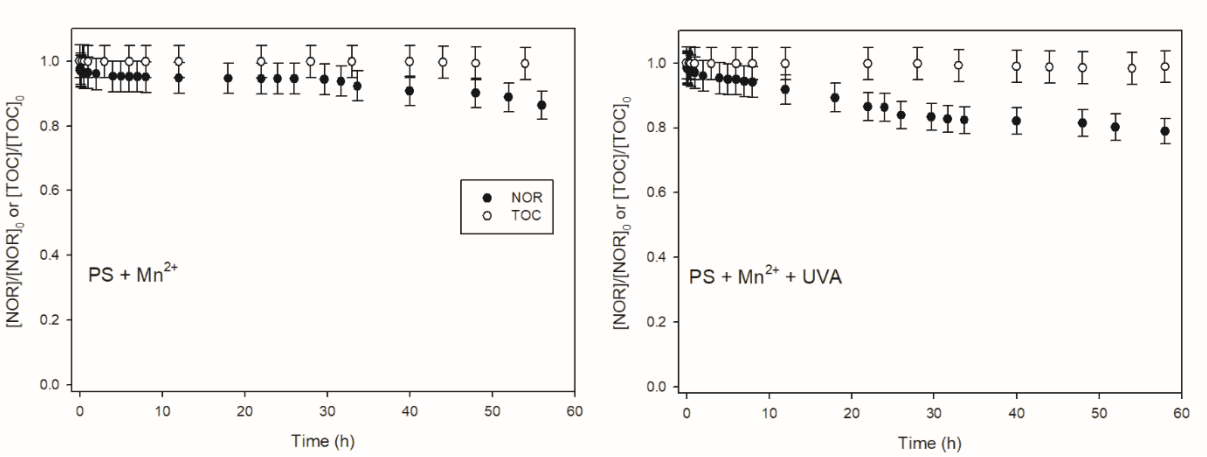

Figure S15. Removal kinetics of NOR (full symbols) and TOC (empty symbols) with Mn^{2+} and $S_2O_8^{2-}$ (PS) under dark and irradiation conditions and at pH 6.5 ± 0.1: $[NOR]_o$ = 24 µM; $[S_2O_8^{2-}]_o$ = 0.5 mM; $[Mn^{2+}]_o$ = 48 µM.

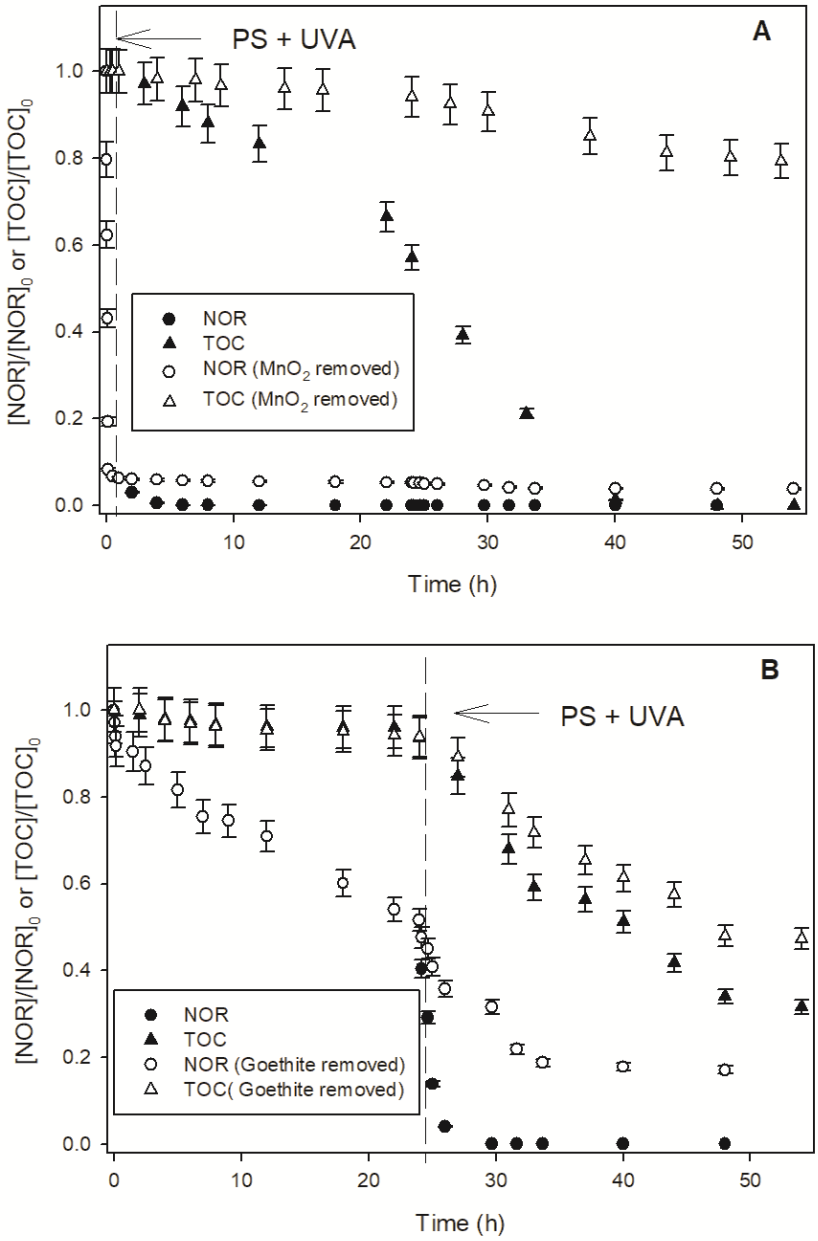

Figure S16. Removal kinetics of NOR_{tot} and TOC_{tot} after removing MnO_2 or goethite after 1 h and 24 h of pre-equilibration time, respectively, at pH 6.5 ± 0.1: $[NOR]_o$ = 24 µM; $[S_2O_8^{2-}]_o$ = 0.5 mM; $[MnO_2]_o$ = 0.027g L^{-1} (10 m^2 L^{-1}); The arrow indicates the moment where oxidant addition and UVA irradiation take place.

Table S1. Reactivity percentage of radicals with species in solution

Radical	Species and concentration	k'' ($M^{-1} s^{-1}$)	k' (s^{-1})	% of reactivity
	FLU (24 µM)	1.2×10^{10}	2.88×10^{5}	4.6
$HO^{\bullet}$	t-But (10 mM)	6.0×10^{8}	6.0×10^{6}	95.3
	PS (0.5mM)	1.2×10^{7}	6.0×10^{3}	< 0.1
	FLU (24 µM)	1.8×10^{9}	4.32×10^{4}	83
$SO_4^{\bullet-}$	t-But (10 mM)	8.4×10^{5}	8.4×10^{3}	16
	PS (0.5mM)	6.5×10^{5}	3.25×10^{2}	< 0.1

The percentage of the hydroxyl radical (•OH) and sulfate radical ($SO_4^{\bullet-}$) reacted with FLU, scavenger and oxidant can be estimated using the bimolecular rate constants and concentration of each species. According to our calculations (Table S1), t-Butanol (10mM) is selective for •OH since it will react with more than 95 % of hydroxyl radical. Isopropanol has been used at high concentration (*i.e.* 100 mM) to ensure effective and total scavenging of hydroxyls radicals.

Table S2. Second order rate constant (*k*) determined using laser flash photolysis experiments between sulfate radical and NOR (initial concentration of 24 µM) at different reaction times (0 - 24h) with MnO_2.

Reaction time	*k* (L mgC^{-1} s^{-1})
0 min	1.66×10^7
6 min	1.57×10^7
1 h	1.57×10^7
24 h	1.56×10^7

Table S3. Main crystallographic data obtained from Rietveld refinements of powder XRD patterns of various MnO_2 samples presented in Figure S13.

Sample	Cell parameters (Å)		Refined *4f* site occupancy (%)	χ^2
	a	c		
MnO_2	4.4026(1)	2.8726(1)	97(2)	2.04
MnO_2 +NOR	4.4028(1)	2.8734(1)	98(1)	3.85
MnO_2 +Mn^{2+}	4.4029(1)	2.8733(1)	98(1)	3.23
MnO_2 + UV	4.4058(2)	2.8752(2)	91(2)	3.34
MnO_2 + NOR + Mn^{2+}	4.4029(1)	2.8735(1)	100(1)	2.52
MnO_2 + NOR + Mn^{2+} + UV	4.4029(1)	2.8732(1)	88(1)	2.89

To check the structural modification of pyrolusite, XRD patterns were recorded for MnO_2 particles undergoing different oxidation reactions (Fig S13). All the patterns are indexed with the expected tetragonal pyrolusite structure (β-MnO_2, space group $P4_2/mm$, no. 136) and an additional peak around 26.6° that can be attributed to the main intensity peak of γ-MnO(OH) (space group $P2_1/c$, no. 14). The main observed differences between the patterns come from the relative intensities of some Bragg peaks (for example (200) and (111) in the inset to Figure S13). Simulation of XRD patterns easily correlates these relative intensity changes to the occupancy of the oxygen *4f* Wyckoff position in the unit cell. XRD thus showed the reduction of MnO_2 under UVA irradiation, inducing oxygen depletion in the pyrolusite structure but yet no visible structural change (e.g. into hausmannite or manganosite) can be determined. Rietveld refinements were performed by including this occupancy as a varying parameter. While no significant deviation from a full occupancy is found for MnO_2 in the presence of NOR, Mn^{2+} or a combination of both, the occupancy drops to about 90 % of its theoretical value when MnO_2 was subjected to UV irradiation (Table S3).